



Wafer-scale replicated gratings for compressing ultrafast laser pulses at telecom wavelengths

FABIAN LÜTOLF,¹  FLORENCE FRIEBEL,² IVAN KUZNETSOV,^{2,3} 
BENJAMIN RUDIN,⁴  FLORIAN EMAURY,⁴  BENJAMIN GALLINET,¹
ROLANDO FERRINI,¹ GUILLAUME BASSET,^{1,*} AND BOJAN
RESAN^{2,5} 

¹CSEM SA, Rue Jacquet-Droz 1, 2002 Neuchâtel, Switzerland

²FHNW University of Applied Sciences and Arts Northwestern Switzerland, School of Engineering, Klosterzelgstrasse 2, 5210 Windisch, Switzerland

³Institute of Applied Physics of the Russian Academy of Science, Uljanov str. 46, 603600 Nizhny Novgorod, Russia

⁴Menhir Photonics AG, Industriestrasse 42, 8152 Glatbrugg, Switzerland

⁵Faculty of Medicine, Josip Juraj Strossmayer University, Josipa Huttlera 4, 31000 Osijek, Croatia

*guillaume.basset@csem.ch

Abstract: Wafer-scale, nanoimprint lithography-based approaches for manufacturing of high-efficiency transmission gratings at telecom wavelengths are reported. Two microns-deep, binary gratings are thereby fabricated and combined with a subwavelength, antireflective structure to achieve a cost-efficient and reliable manufacturing process. Diffraction efficiencies of 92% are experimentally achieved in the Littrow configuration. These gratings are used to compress 8 picosecond pulses with 1W of average output power at central wavelength of 1555nm to pulse duration of 378 femtoseconds

© 2022 Optica Publishing Group under the terms of the [Optica Open Access Publishing Agreement](#)

1. Introduction

Grating based laser compressors have been extensively studied in the last 30 years and are still the most popular tool for generating high-power, ultrashort laser pulses using chirped pulse amplification (CPA) [1–3]. In this method the pulse is first stretched in time, amplified and then compressed [1,4–6]. The centerpiece of such a compressor is a high-efficiency diffraction grating with the rest of the mirrors and lenses built around it. Various routes for manufacturing of such high-efficiency gratings have been established like ruling [7,8], laser interference/holography [9] or direct writing by an electron / laser beam followed by reactive ion etching (RIE) [10,11] and potential (oblique) evaporation to increase the efficiency [12]. In the case of a transmission setup, an additional antireflective (AR) coating is required. Unfortunately, these technologies are relatively expensive due to their long processing time and expensive equipment used, as well as possible inhomogeneities on a wafer area. Substantial efforts have therefore been taken in the past to reduce the manufacturing costs of high efficiency gratings [11]. One possibility is utilizing nanoimprint lithography (NIL) processes [13]. These processes offer high reproducibility and possibility for high to very high throughput, as well as good process control while requiring much less sophisticated equipment and shorter process times compared to plasma etching processes [14]. NIL processes still rely on a so-called master structure, which is the template used as a mold for replication, but the above-mentioned advantages then apply to each copy made from this master. Deep or slanted grating nanostructures however are challenging to replicate on large areas. However, many efficient grating designs rely on such nanostructures [15,16]. Furthermore, these structures are often tailored to a very limited wavelength range and adapting them to different wavelength ranges is difficult.

We are presenting two NIL-based routes for fabricating efficient transmission gratings that rely on deep binary gratings. The first route (A) provides a simple, cost effective and reliable way to produce a series of high efficiency diffraction gratings from a master template. Such gratings will be identical to their template and will not have tunable properties. The route B offers a much higher flexibility in the fabrication of very high efficiency diffraction gratings. It involves more complex process steps but have lighter requirements for the grating replication process and wavelength range tunability. The diffraction properties attainable through these routes are first assessed in Rigorous Coupled Wave Analysis (RCWA, [17,18]) simulations. It is shown that not only a peak efficiency of $>97\%$ is achievable at 1550nm wavelength for an optimized grating geometry, but that efficiencies of $>96\%$ can be accomplished throughout most of the telecom wavelength bands by simple tuning of the grating depth. Both fabrication routes are subsequently tested and used to manufacture gratings on full 5-inch wafers with $>92\%$ diffraction efficiency at 1550nm wavelength, which is the most common wavelength for telecommunication related applications [19,20]. The resulting quality of the gratings is finally assessed by including them in a laser compressor and demonstrating femtosecond pulse compression at this exact wavelength [21].

2. Materials and methods

2.1. Simulations

RCWA simulations were performed on the model visible in Fig. 1(c). The refractive index of the grating material, the sol-gelOrmocomp, was approximated by 1.52, which is the datapoint available at 589nm. Data for 1550nm wavelength was not available but the dispersion is expected to be reasonably low, and the attainable efficiency is not extremely sensitive to the refractive index (RI). Even for significantly lower RI material like for example fused silica, simple adaptation

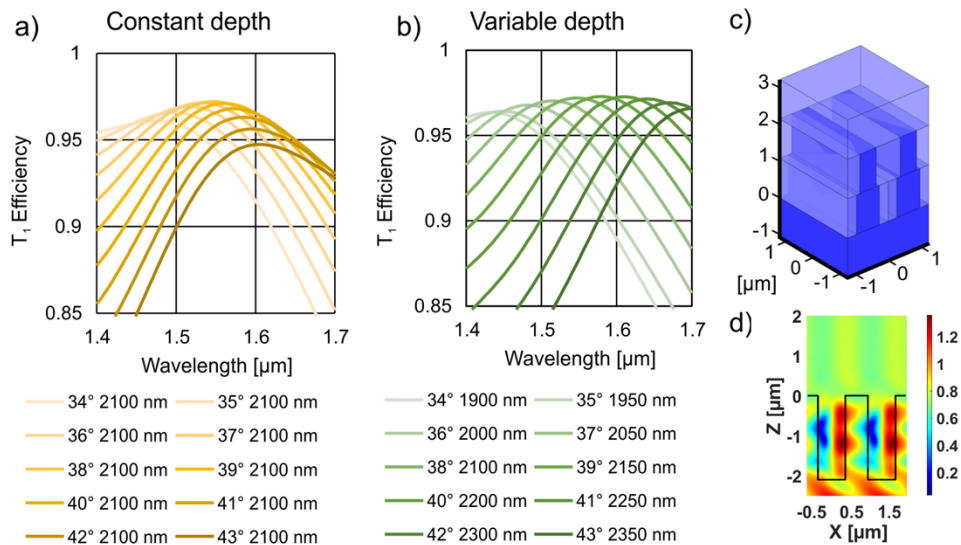


Fig. 1. RCWA simulation of 1st order diffraction efficiencies for s-polarized light of a grating having a 1250 nm period with a) constant depth and b) variable depth at different AOI. c) shows 2 periods of the simulation model, the dark blue material is the replicated grating in Ormocomp and the light blue material is air. d) FDTD simulation results of the typical time-average electric field intensity in two periods of the grating structure, black line representing the grating profile, illuminated in the transmission Littrow configuration.

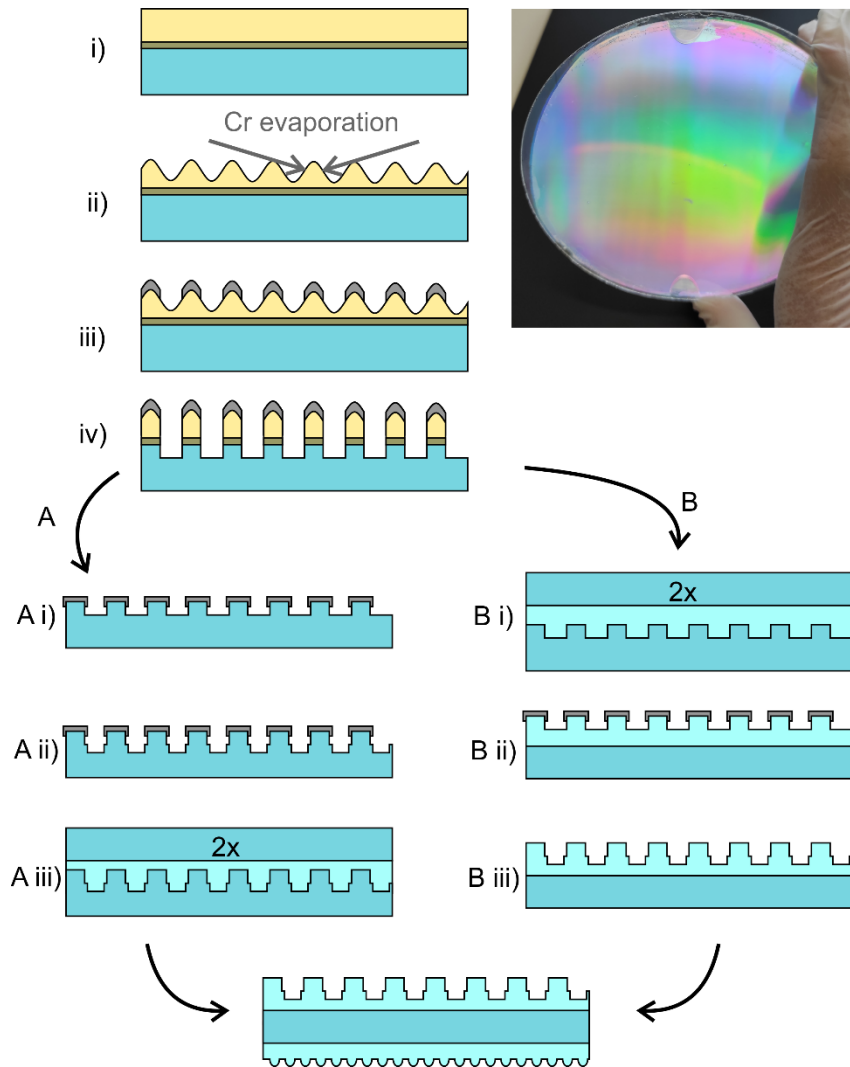


Fig. 2. Schematic detailing the two fabrication routes. Inset: Fully processed 5-inch wafer

of the grating depth can compensate for the deviation (Fig. 2). The absorption of Ormocomp at 1550nm is approximated by zero. Additionally, Finite Differences in Time Domain (FDTD) simulations using Lumerical software were performed on a slanted version of the model using a smaller discretization.

2.2. Fabrication

The process is summarized in Fig. 2. The replication masters were fabricated by laser-interference-lithography: a 5-inch quartz wafer was coated with AZ Barli II-200 (Microchemicals) at 2000rpm on which a 550nm thick layer of S1805G2 Photoresist (Microposit) was spin-coated. The resist was exposed in a dual beam interferometer utilizing a HeCd laser at 441.6nm wavelength (Plasma JSC). Exposure time and development time were iteratively optimized to record a grating of circa 510nm depth in the resist. The grating was subsequently evaporated with 100nm of Chromium (Cr) at an angle of 79° with respect to the surface normal from the two directions perpendicular

to the grating lines. The residual layers of photoresist and Barli II were removed in oxygen reactive ion etching plasma (Plasmalab 80 plus) before transferring a rectangular profile into the quartz (Oxford Plasma Pro 100 Cobra, 150W RIE and 1500W ICP, 5mTorr, 5', 20sccm C₄F₈, 100sccm Ar). The chromium was removed by immersion in Chrome Etchant 18 (Microresist Technologies) and subsequently cleaned in Nanostrip. For the deeper grating, the process was repeated with a different CR evaporation angle (45°) and an etching time of 4min. Etching into the sol-gel replication material (Ormocomp) was done with the same machine but with 200W RIE at 20mTorr; and 10sccm CHF₃ / 40sccm Ar for 4min 15s.

The molds of the diffraction gratings were done by replicating the master into Polyurethane on a standard 5-inch glass substrate. The mold was teflonized (sputtered at 4.6×10^{-2} mbar in CHF₃ atmosphere, 50W RF) before treatment with BGL-GZ-83 (Profactor) for anti-adhesion. The mold was subsequently used to replicate the final structure in Ormocomp (Microresist) on a D263T glass (Schott). The replication process was identical for the antireflective (AR) structures on the other wafer side, apart from the mold material which was Ormocomp instead of Polyurethane and the grating being protected with an AZ 40XT-11D (Microchemicals) resist layer during this process.

3. Results

3.1. Grating simulation and fabrication results

RCWA simulations have been performed to optimize the transmittance into the first diffraction order (T_1) of a 1250nm period grating in Littrow configuration for s-polarized light. Littrow configuration is achieved when the first diffraction order is redirected towards the incident beam for a reflective grating, while input and output angles are the same for the transmission grating. In our case, this case can be observed at 38.3° angle of incidence (AOI) with respect to the grating plane for the target wavelength of 1550nm. The equation below shows the relation between these values:

$$\theta_m = \sin^{-1} \left(\frac{n_1 \sin(\theta_i) + m \frac{\lambda}{\Lambda}}{n_2} \right) \quad (1)$$

where θ_m is the output angle for order m , n_1 is the refractive index of the incident medium, n_2 the refractive index of the material the outgoing beam propagates in, θ_i the angle of incidence, Λ the grating period, and λ the vacuum wavelength. Littrow configuration for the m^{th} order occurs for $\theta_m = \theta_i$. It was found that a simple binary grating with a duty cycle (width of the grating ridge divided by the grating period) of 40% and a depth of 2100nm could achieve >97% first order diffraction efficiency in this configuration (Fig. 1(a)), which is close to typical holographic gratings available commercially [22]. The simulation model is shown in Fig. 1(c) with a refractive index of 1 for the incidence in air and of 1.52 for the substrate.

A small taper was introduced to account for the light sidewall inclination observed for the etching process utilized in this study (Fig. 3(b)). In Fig. 1(a), the chosen grating shows a pronounced maximum at the target wavelength of 1550nm and 38° AOI, which is the geometry it has been optimized for. Even though the efficiency is broadband in wavelength, a clear deterioration of the efficiency is observed when the grating is operated outside of these optimal conditions. Efficiencies of approximately 92% can be achieved at 1700nm wavelength and the corresponding Littrow angle of approximately 43° (darkest yellow line). It is also clearly visible that, even though at 1700nm wavelength the Littrow angle is at 43° AOI, the peak efficiency is found around 1600nm in this configuration. To improve the efficiency at wavelengths away from the main design wavelength of 1550nm, it was found that a possible solution is to increase the grating depth while keeping all the other parameters as in Fig. 1(a). With this simple adaptation, efficiencies >96% can be achieved in the entire wavelength range as confirmed by the green curves in Fig. 1(b). The physical explanation for this observation can be found by investigating the

optical near-field. Figure 1(d) shows a simulation of the near-field intensity at 1560nm performed with the FDTD software Lumerical, supported by a time-domain movie, [Visualization 1](#), of the propagating electric field in supplementary information. The field in the grating pillars is mainly distributed in two zones: a low-intensity zone with a phase discontinuity, and a high-intensity zone with a phase delay from the incident field. The magnitude of the phase delay depends on the optical path difference between light propagating in the pillar and in the environment. This is confirmed by the presence of an optimal efficiency at a given grating depth.

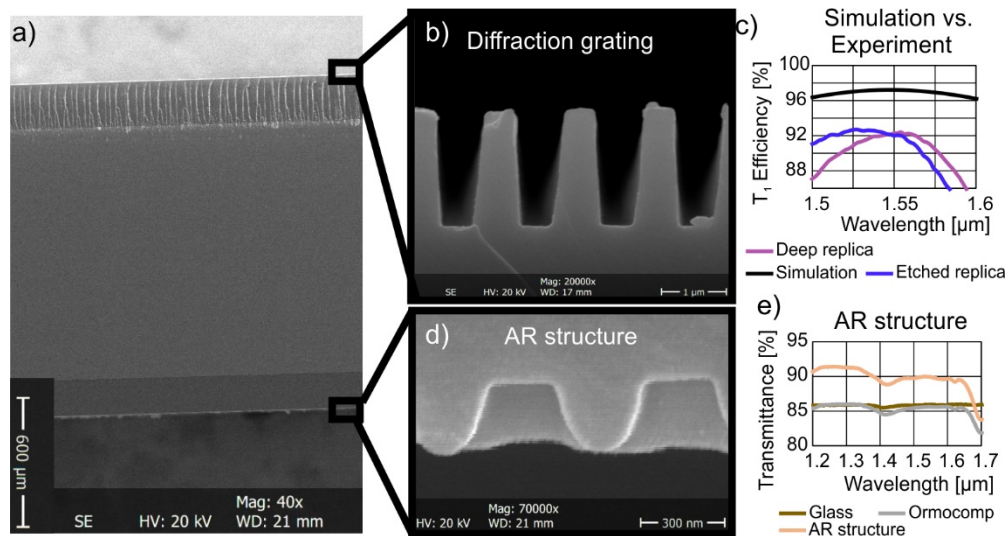


Fig. 3. Scanning Electronic Microscopy (SEM) pictures of a) the full wafer, b) the front side diffraction grating and d) the backside AR structures. The measured diffraction efficiency of the full device in c) and the transmittance of the AR structures replicated in Ormocomp compared with the bare glass and the Ormocomp coated glass in e)

Note that, even though the observed efficiency-drop of approximately 4% from 96% to 92% seems minor, the difference accumulates during the 4 passes in a pulse compressor configuration. If the overall compressor efficiency amounts to 85% for a grating with 96% efficiency, it drops to approximately 72% for a grating with 92% efficiency. It is finally worth mentioning that for wavelengths around 1300nm (O telecommunication band), the deeper gratings of 2000nm – 2100nm depth are suitable again and show efficiencies around 96% (Figure S1). At 1270nm, the -2^{nd} order appears for $n_2 = 1.52$. This so-called Wood-Rayleigh anomaly [7,23–25] causes a kink in the spectrum as light is redistributed into this additional order for lower wavelengths.

In summary, the above findings suggest to either only work with a single wavelength and fully optimize the grating for this wavelength, including the grating period and depth, or to adapt the grating depth according to the targeted wavelength range. In the following, we propose a replication-based fabrication process that could accommodate either of these goals depending on its implementation (Fig. 2).

As for all replication processes, the starting point is the generation of a master structure. In this work, we used laser interference lithography as it can produce homogeneous grating structures over large areas in a single exposure (Fig. 2(i) and (ii)). The resulting sinusoidal grating is coated obliquely with Cr (iii), which acts as a hard mask for the subsequent reactive ion etching (RIE). A first oxygen RIE removes the residual resist layers and a second CHF₃ RIE transfers the binary grating into the quartz substrate (iv). After removing the Cr mask as well as the remaining resist by photoresist stripping and chromium wet etching, a binary master grating with

limited depth/efficiency is produced. Two options are available to replicate and improve this master: Route A continues by redepositing Cr obliquely on the grating-patterned quartz (A i) and performing a 2nd CHF₃ RIE to deepen the grating (A ii). After removing the chromium, this deep grating can subsequently be replicated by utilizing an elastomeric Polyurethane (PU) mold. PU is sufficiently elastic to facilitate release of the deep structures while being rigid enough to prevent them from collapsing or changing shape when molding the uncured Ormocomp sol-gel. The PU mold is used to replicate the grating using nanoimprinting into the final Ormocomp material (A iii), a hybrid organic-inorganic sol-gel material by ultraviolet (UV) nanoimprinting. Ormocomp is more durable than organic materials and matches the refractive index of the glass substrate. Route B proceeds by replicating the shallower grating into a Polyurethane mold, which is then used to produce a nanoimprinted replica in Ormocomp material (B i). This Ormocomp grating replica is coated with a Cr hard mask (B ii) and etched (CHF₃ RIE) to the desired depth before the Cr is removed by wet etching (B iii).

For both routes, the device is finalized by replicating an antireflective (AR) nanostructure on the backside of the substrate using again nanoimprinting with an Ormocomp material, which is cost efficient. This step is necessary to use the grating in the first order of diffraction in transmission and to achieve a high compressor efficiency. In this study, a two-dimensional grating was used with a period of 550nm and 350nm peak to valley depth as AR structures.

Route A can hence be used to produce gratings of constant depth with very high reproducibility. The simplicity, cost and reliability of the process bring clear advantages. Route B offers the option of adapting the depth after replication, but at the expense of an additional oblique vacuum Physical Vapor Deposition (PVD) and RIE step. On the other hand, route B has lighter requirements on the replication process, as the grating is much less deep at the time of replication and has the potential of achieving even higher aspect ratios if required after RIE.

Both process routes were tested and could successfully be implemented on full 5-inch wafers (Fig. 2, inset). The resulting grating shape for both routes was very similar and close to the design (Fig. 3(a),(b), see also Figure S3 for more details). Efficiencies of 92% in the first diffracted order in transmittance could be reached for both routes (Fig. 3(c)), with a minor depth difference of 150nm that explains the slightly different measured efficiency spectra.

Even though measurements are below the theoretical limit, they are very good considering they stem from a fully replicated 5-inch wafer. The largest contribution to this gap between simulation and fabricated devices results from the AR structures (Fig. 3(d)) which increase transmittance by 4.3% (Fig. 3(e)) only. The reflectance per interface according to Fresnel's formulas would be 7.6% for s-polarized light so an increase by another 3.3% would be possible with fully optimized AR structures. Optimization of the AR structures would however go beyond the scope of this publication. Many different AR structures from moth-eye inspired nano-pillars to nano-pyramids have been reported elsewhere [26–28] and can be replicated instead of the 2D grating utilized here. An additional difference of diffraction efficiency of 1.7% between the simulated and experimental measurements are likely caused by fabrication imperfections, sol-gel absorption and possibly scattering and slight deviations from the simulated design. This low level of loss in efficiency emphasizes the high process control and reliability of the fabrication chain for the main diffraction grating as well as the low shrinkage of the Ormocomp material during UV reticulation.

Note that care must be taken to the choice of nanoimprint material and substrate: their refractive indices have to match to prevent any reflection at their interfaces and no absorption bands should occur at the wavelengths of interest. With the Ormocomp material, the refractive index matches very well as virtually no difference in transmittance is observed between the bare glass and the same glass with a layer of Ormocomp attached (see Fig. 3(e)). The selected Ormocomp introduces no absorption losses for the main telecom wavelengths around 1550nm and 1300nm,

but it would need to be substituted for applications around 1400nm or 1700nm due to well visible absorption bands.

3.2. Grating validation in compressor of femtosecond pulses

Finally, we demonstrate the pulse compression of an amplified laser with the new produced gratings. A folded grating compressor with a MENHIR-1550 laser oscillator (Menhir Photonics) as a light source at 1550nm wavelength was used for this proof of principle experiment. The 250fs output pulses of this oscillator have been stretched in a 20m passive optical fiber before the fiber amplifier to serve as an input for our compressor setup with 38° angle of incidence on the grating.

We used a folded Martinez type compressor setup [29]. The setup is depicted in Fig. 4. From the compact laser source, the beam is sent through the compressor as illustrated in the Fig. 4, on the right. In this configuration, after the grating, the pulse is sent to a curved mirror ($f = 200\text{mm}$). In the focal plane of that mirror, a plane mirror is placed to enable the four passes through the grating. From there, the pulse is sent back to the curved mirror and to a roof top mirror.

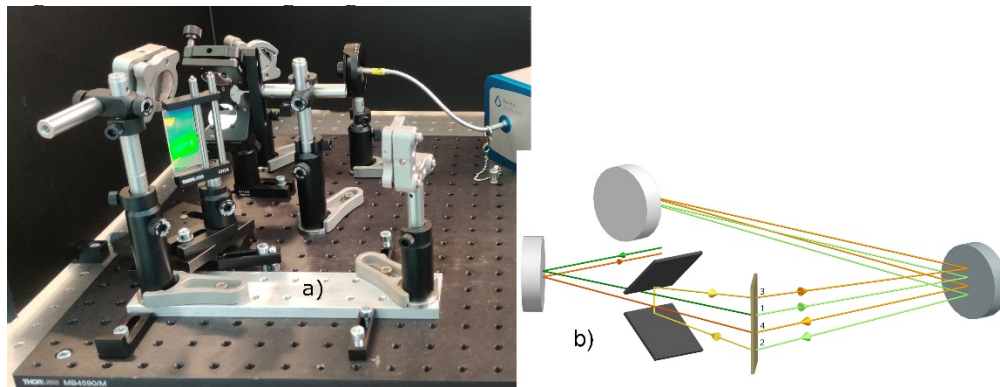


Fig. 4. On the left a) is the experimental setup with the 1550 nm laser oscillator from Menhir Photonics and the compact setup of the folded Martinez-type compressor [26]. Shimmering green in this image is the grating produced by CSEM. On the right b) is the schematic of the four beam passes through the grating in the compressor. The input is dark green, and the first pass and the second pass through the grating are lime green. The orange-colored lines are representing the third and fourth pass through the grating.

We measured the performance of the compressor setup with an input of 1.12W average power and 8 picosecond pulse duration after the fiber amplifier. First, we confirmed 92% diffraction efficiency for a single pass through the grating. The laser output pulses after compressor are temporally measured with a second-harmonic generation (SHG) autocorrelator, as in Fig. 5(b). The measured SHG autocorrelation FWHM is 584fs, corresponding to 378fs deconvolved pulse duration, assuming a sech^2 temporal shape. The spectrum of the compressed output pulse has been measured with an Optical Spectrum Analyser (Ando, AQ6317, with set resolution to 2nm) yielding 12nm optical bandwidth at FWHM. The calculated time-bandwidth product is 0.57, which is somewhat larger than the theoretical minimum value of 0.315 for sech^2 transform limited pulses. The larger value is caused mainly by non- sech^2 pulse and spectrum profile, and by uncompressed higher order dispersion in pulses coming from the fiber amplifier.

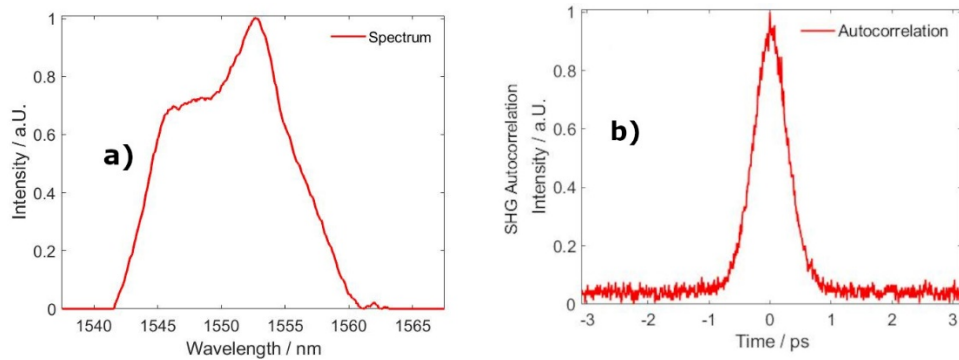


Fig. 5. a) The spectrum after the compressor and b) the SHG autocorrelation trace of 378fs pulse duration obtained with 1W of average output power from the source.

4. Conclusion

In summary, new fabrication methods for high efficiency diffraction gratings have been presented. After a master structure is fabricated using interference lithography, oblique PVD and RIE, the gratings are replicated using UV nanoimprint lithography with a robust solgel material,Ormocomp, on full 5" wafers. The ~ 2 microns deep grating structures with a period of 1250nm are replicated with very good fidelity to the master and demolded without difficulties and with good reproducibility by using a polyurethane elastomeric mold. This process provides an affordable cost per gratings with 97% reachable diffraction efficiencies, close to the ones of etched quartz, by requiring no or minimal RIE for each grating replication. Two different designs strategies are elaborated and different trade-offs between flexibility and process cost are evaluated using RCWA and fabrication options. The two presented grating manufacturing routes are very attractive in terms of reproducibility, as well as cost-efficiency, while achieving a comparable diffraction efficiency to conventional quartz gratings. The high efficiency of 92% of our replicated gratings in transmission is demonstrated experimentally by diffraction efficiency measurement in an ultrafast pulse compressor. The discrepancy between numerical modelling and experimental is due to non-optimized NIL replicated anti-reflective coating and multiple options exist to improve the anti-reflections structures as reported in [26–28]. The NIL-based gratings were built into a Martinez type folded compressor and picosecond pulse compression to close to bandwidth-limited pulses in the fs-regime could be demonstrated with the laser at 1555nm wavelength, delivering 1W of average output power. The compressed pulse duration was 378fs from a spectral bandwidth of 12nm, corresponding to 0.57 time-bandwidth product. The demonstration of this design and fabrication method at other wavelengths such as 1030nm will require to modify the design and adapt the process parameters.

Funding. Swiss Nanoscience Institute (Nanoargovia grant 14.19).

Acknowledgements. The authors acknowledge the support from Femtoeasy for the use of their pulse measurement device.

Disclosures. BR and FE: Menhir Photonics (I,E). The other authors declare no conflict of interests.

Data availability. Data underlying the results presented in this paper are not publicly available at this time but may be obtained from the authors upon reasonable request.

Supplemental document. See [Supplement 1](#) for supporting content.

References

1. D. Strickland and G. Mourou, "Compression of amplified chirped optical pulses," *Opt. Commun.* **56**(3), 219–221 (1985).

2. C. Zhou, "Chirped pulse amplification: review and prospective from diffractive optics [Invited]," *Chin. Opt. Lett.* **18**(11), 110502 (2020).
3. A. M. Weiner, "Femtosecond pulse shaping using spatial light modulators," *Rev. Sci. Instrum.* **71**(5), 1929–1960 (2000).
4. E. Treacy, "Optical pulse compression with diffraction gratings," *IEEE J. Quantum Electron.* **5**(9), 454–458 (1969).
5. S. Backus, C. G. Durfee, M. M. Murnane, and H. C. Kapteyn, "High power ultrafast lasers," *Rev. Sci. Instrum.* **69**(3), 1207–1223 (1998).
6. W. Sibbett, A. A. Lagatsky, and C. T. A. Brown, "The development and application of femtosecond laser systems," *Opt. Express* **20**(7), 6989–7001 (2012).
7. R. W. Wood, "XLII. On a remarkable case of uneven distribution of light in a diffraction grating spectrum," *The London, Edinburgh, and Dublin Philosophical Magazine and Journal of Science* **4**(21), 396–402 (1902).
8. X. Mi, S. Zhang, X. Qi, H. Yu, H. Yu, and Y. Tang, "Ruling engine using adjustable diamond and interferometric control for high-quality gratings and large échelles," *Opt. Express* **27**(14), 19448–19462 (2019).
9. J.-H. Seo, J. H. Park, S.-I. Kim, B. J. Park, Z. Ma, J. Choi, and B.-K. Ju, "Nanopatterning by Laser Interference Lithography: Applications to Optical Devices," *J. Nanosci. Nanotechnol.* **14**(2), 1521–1532 (2014).
10. A. Schilling, P. Nussbaum, I. Philipoussis, H. P. Herzig, L. Stauffer, M. Rossi, and E.-B. Kley, "Fabrication technologies for micro-optical elements with arbitrary surfaces," in *Micromachining Technology for Micro-Optics* (SPIE, 2000), Vol. 4179, pp. 65–72.
11. P. Lalanne, S. Astilean, P. Chavel, E. Cambriil, and H. Launois, "Blazed binary subwavelength gratings with efficiencies larger than those of conventional échelle gratings," *Opt. Lett.* **23**(14), 1081–1083 (1998).
12. F. Lütolf, M. Stalder, and O. J. F. Martin, "Up-scalable method to amplify the diffraction efficiency of simple gratings," *Opt. Lett.* **39**(23), 6557–6560 (2014).
13. H. Lan and Y. Ding, *Nanoimprint Lithography* (IntechOpen, 2010).
14. H. Thiele, M. T. Gale, C. Gimkiewicz, S. Mahmud, J. Sochtig, S. Westenhofer, and Ch. Zschokke, "Replicated Micro-Optic Chirped Grating Waveguide Coupler for Data/Telecom Monitoring Applications," in *2002 28TH European Conference on Optical Communication* (2002), Vol. 4, pp. 1–2.
15. T. Levola and P. Laakkonen, "Replicated slanted gratings with a high refractive index material for in and outcoupling of light," *Opt. Express* **15**(5), 2067–2074 (2007).
16. S. Wang, C. Zhou, Y. Zhang, and H. Ru, "Deep-etched high-density fused-silica transmission gratings with high efficiency at a wavelength of 1550 nm," *Appl. Opt.* **45**(12), 2567–2571 (2006).
17. M. G. Moharam and T. K. Gaylord, "Rigorous coupled-wave analysis of planar-grating diffraction," *J. Opt. Soc. Am.* **71**(7), 811–818 (1981).
18. K. Knop, "Rigorous diffraction theory for transmission phase gratings with deep rectangular grooves," *J. Opt. Soc. Am.* **68**(9), 1206–1210 (1978).
19. R. Paschotta, S. C. Zeller, S. Lecomte, U. Keller, L. Krainer, G. J. Spühler, and K. J. Weingarten, "Pulse generating lasers for telecom applications," in *Frontiers in Optics* (2003), Paper WJJ3 (Optical Society of America, 2003), p. WJJ3.
20. I. Pavlov, E. Ilbey, E. Dülgergil, A. Bayri, and F. Ö. Ilday, "High-power high-repetition-rate single-mode Er-Yb-doped fiber laser system," *Opt. Express* **20**(9), 9471–9475 (2012).
21. L. Lefort, J. H. V. Price, D. J. Richardson, G. J. Spühler, R. Paschotta, U. Keller, A. R. Fry, and J. Weston, "Practical low-noise stretched-pulse Yb³⁺-doped fiber laser," *Opt. Lett.* **27**(5), 291–293 (2002).
22. K. Buchwald, *Fused Silica Transmission Gratings* (Ibsen Photonics, 2007).
23. L. Rayleigh, "III. Note on the remarkable case of diffraction spectra described by Prof. Wood," *The London, Edinburgh, and Dublin Philosophical Magazine and Journal of Science* **14**(79), 60–65 (1907).
24. L. Rayleigh, "On the dynamical theory of gratings," *Proc. R. Soc. Lond. A* **79**(532), 399–416 (1907).
25. D. Maystre, "Theory of Wood's anomalies," In: *Plasmonics: From Basics to Advanced Topics*, (Springer, 2012), Vol. 167.
26. C. David, P. Häberling, M. Schnieper, J. Söchtig, and C. Zschokke, "Nano-structured anti-reflective surfaces replicated by hot embossing," *Microelectron. Eng.* **61-62**, 435–440 (2002).
27. H. K. Raut, V. A. Ganesh, A. S. Nair, and S. Ramakrishna, "Anti-reflective coatings: A critical, in-depth review," *Energy Environ. Sci.* **4**(10), 3779–3804 (2011).
28. C. Zhang, P. Yi, L. Peng, and J. Ni, "Optimization and continuous fabrication of moth-eye nanostructure array on flexible polyethylene terephthalate substrate towards broadband antireflection," *Appl. Opt.* **56**(10), 2901–2907 (2017).
29. O. Martinez, "3000 times grating compressor with positive group velocity dispersion: Application to fiber compensation in 1.3–1.6 μm region," *IEEE J. Quantum Electron.* **23**(1), 59–64 (1987).